Plasma Sources Sci. Technol. **24** (2015) 035009 (7pp) doi:10.1088/0963-0252/24/3/035009

Plasma parameters of the hollow cathode magnetron inside and downstream

N P Poluektov, Yu P Tsar'gorodsev, I I Usatov, A G Evstigneev and I A Kamyschov

Department of Physics, Faculty of Electronics, Moscow State Forest University, 141005 Mytischi-5, Moscow Region, Russia

E-mail: poluekt@mgul.ac.ru

Received 12 November 2014, revised 23 March 2015
Accepted for publication 27 March 2015
Published 7 May 2015

Absract

This paper deals with the characterization of ionized physical vapour deposition (IPVD) by means of a hollow cathode magnetron (HCM). The pressure is 10 mTorr with 2.2 kW discharge power. A Langmuir probe was used to study the spatial distribution of plasma parameters such as the electron density and temperature, electron energy distribution function, plasma space and floating potentials inside and outside the HCM. It was found that the high density plasma inside the cathode occurs near the side surface in the ionization region. The plasma density on the axis is reduced. The EEDF shows the presence of electrons with energy up to 30 eV. The measurements showed that ionization occurs not only within the cathode but also outside. The magnetic trap placed around the anode ring increases the density and homogeneity of the plasma several times in the region of its location.

Keywords: hollow cathode magnetron, ionized physical vapor deposition , Langmuir probe diagnostic

(Some figures may appear in colour only in the online journal)

1. Introduction

Hollow cathode magnetrons (HCMs) are the plasma sources used for film deposition using metal atoms and ions. The HCM's cup-shaped target geometry electrostatically and magnetically confines electrons within the volume of the source so that losses are minimized. As a result, a high-density plasma (up to 10^{12} cm^{-3}) is created inside the HCM and also at large distances from the source. The characteristic difference between this technique and conventional approaches is that a high fraction of the sputtered material is ionized, while in traditional magnetron sputtering, the sputtered species are almost exclusively neutral. The ionized physical vapor deposition (IPVD) method is increasingly used to deposit diffusion barriers and copper seed layer materials onto high-aspect ratio vias and trenches for microelectronics fabrication [1–5].

Several techniques have been developed for obtaining an ionized growth flux. The plasma may be generated, for example, by inductively coupled radio-frequency (rf) power [3–5] or by electron cyclotron resonance [6]. In recent years, high-power impulse magnetron systems (HIPIMS) have been used for deposition of films. The peak plasma density during the active cycle of this discharge exceeds 10^{12} cm^{-3} and the degree of ionization of sputtered metal atoms reaches 80% [7–9].

An HCM uses a single dc power supply to both sputter and ionize the target material, unlike other IPVD tools that use secondary inductively coupled or ECR plasma sources for ionization of sputtered atoms. HCMs have been investigated both experimentally and via computer modeling [1, 2, 10–12] but many phenomena remain unclear. In particular, to our knowledge, measurements of plasma parameters inside the HCM have not been performed. To better understand the fundamental mechanisms of the HCM it is desirable to study processes occurring within this ionization region.

The purpose of this paper is to study plasma parameters inside the HCM and downstream. To do this the spatial distribution of plasma parameters of the HCM were studied using probe techniques.

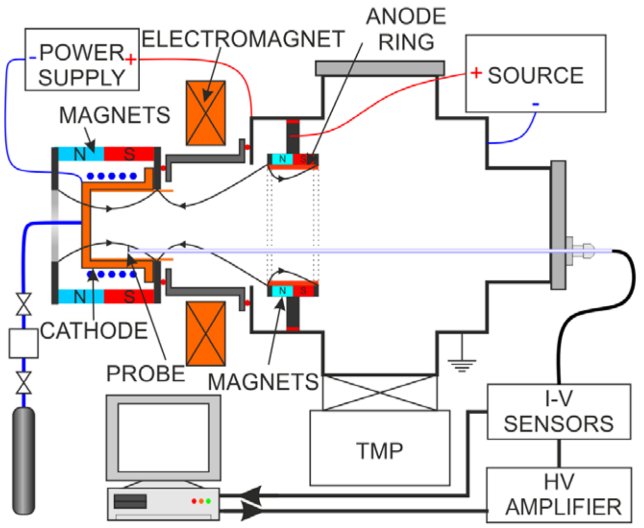

Figure 1. The experimental setup.

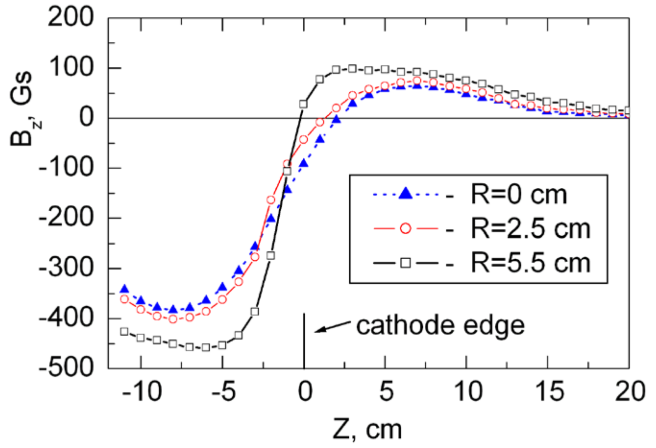

Figure 2. The magnetic field B_z along Z axis at various radii. I_{el} = 3.5 A.

2. Experimental apparatus

The experimental setup of the magnetron discharge with a hollow cathode is shown in figure 1 [12]. The cathode consists of a cup-shaped Cu target (diameter 0.14 m, length 0.11 m) made of copper and cooled with water. The HCM is powered by the inverter source, providing up to 12 kW. The chamber was pumped to base pressure $5{\cdot}10^{-6}$ Torr using a turbomolecular pump (700 l s^{-1}) backed up with a rotary pump (60 m^3 h^{-1}). The target was sputtered using argon gas with pressure 10 mTorr measured using a Baratron pressure gauge positioned 400 mm from the target. The operation pressure was maintained by adjusting the pumping rate via a throttle valve. Gas flow (50 sccm) is provided by a gas flow controller.

Geometry of the magnetic field inside the cathode in these experiments was chosen to be fairly simple in order not to complicate the already difficult phenomena in the plasma. The magnetic field is produced by eighteen columns of Nd–Fe–B magnets $18 \times 20 \times 140$ mm^3 surrounding the target, with ring iron flanges on the edges. The electromagnet is located downstream of the HCM, and its magnetic field is opposite polarity to that of the permanent magnets. Consequently the magnetic field has a cusp at the mouth of the cathode. Figure 2 shows the longitudinal magnetic field B_z at various radii, measured by a Hall sensor. The magnetic field at the axis is 400 gauss, while near the cylindrical surface of the cathode the field is 450 gauss.

To reduce radial plasma losses, an insulated cylindrical insert of diameter of 180 mm and length 110 mm is mounted between the cathode and reactor. The discharge anode is a copper ring positioned in the reactor and insulated from it. In the experiments described below, a voltage of +20 V was applied to this ring anode from an additional source; in this case, the anode collected the entire discharge current. Around the anode ring are mounted permanent magnets with ring iron flanges on the edges. Their magnetic field is directed opposite to the field of the electromagnet, thus creating a trap near the anode ring.

The substrate in these experiments was not installed.

The electron temperature T_e, electron energy distribution function (EEDF), electron density N_e, floating probe potential U_f and plasma potential U_s were determined from probe measurements. The probe tip of the longitudinal probe was made of a tungsten wire with radius r_p = 0.1 mm and was 4.5 mm long. To reduce the influence of the magnetic field, the probe tip was set normal to the magnetic field lines. At a magnetic field strength 450 gauss, the Larmor radius of electrons with $T_e \sim 6$ eV is $r_L \sim 0.22$ mm. According to Rubinstein and Laframboise [13], for $\beta = r_p/r_L = 0.5$ the electron current is decreased at plasma potential by a factor of 0.9 and the electron saturation current is unaffected if the normalized potential is higher than 2. This was taken into account in the determination of electron density.

In magnetron systems, a significant drift velocity of electrons exists in the $E \times B$ direction, which is the azimuthal direction in our case. Sheridan [14], by means of a one-sided planar Langmuir probe, found that the drift velocity was most significant close to the cathode, whereas further from the cathode it drops off to nominal values with respect to plasma thermal velocities. It has been shown that this flow of plasma can affect the shape of the characteristic obtained, leading to incorrect electron temperatures and plasma potentials. However, the probe only picks up drift velocity components that are perpendicular to the probe surface. We set the probe tip along the azimuthal axis in the direction of $E \times B$ drift. The probe signal is not changed when it is rotated by 180°.

The probe tip was encased in ceramic tubes with 0.4 mm i.d. and 2 mm o.d. A similar probe was used to measure the radial distribution of plasma parameters 19 cm from the cathode exit. Probe measurements in this plasma are not a simple task, due to metal deposition on the probe. Power discharge was 2.2 kW and metal flux was large. This issue was considered in detail in article [10].

Therefore we created a system for rapid recording of probe characteristics. The I–V characteristics were recorded with the help of a PCI card National Instruments NI6221 with a 16-bit ADC, a 16-bit DAC, and multiplexer. The ADC and DAC were connected to a probe via isolated modules. The DAC voltage was increased by a self-made powerful voltage amplifier (with an output voltage range from −80 to +80 V at an output current of up to 500 mA and a voltage rise time of up to $10\,\mathrm{V\,s^{-1}}$). The *I–V* characteristic includes up to 640 pairs. In dense plasma the number of points is fewer (470–540) as the voltage range is limited to the right due to a large electron saturation current, or due to the breakdown probability inside the target. To improve the accuracy of measurements, each pair of current–voltage points is obtained by averaging a set of 10 data points. The time required to obtain one *I–V* curve is about 2 s. To reduce contamination of the probe, the discharge was turned on for a few seconds. After a few measurements the probe was moved to a great distance away from the source and was biased at −180 V to sputter clean the probe tip's surface.

The programs used for data acquisition and processing were written in LabView. The processing program works interactively using the graphical interface and allows for numerical experiments on the data. First the data are smoothed by B-splines or Savitzky–Golay filter, then the plasma potential and electron energy distribution function (EEDF) $f(E)$ are calculated from the first and second derivatives respectively. In the high-density plasma of the HCM discharge the ratio of probe radius to Debye radius is about 5–10, therefore analytical Langmuir theory is not applied for the probe analysis. The electron density is calculated by two methods: by integration of the EEDF and from parametrization of numerical results of the Laframboise theory [15]. The algorithm used is developed from the method described in [16]. Results of these methods agree to within 10%. The electron temperature is defined as average temperature:

$$T_e = \frac{2}{3k} \frac{\int_0^\infty E f(E)\mathrm{d}E}{\int_0^\infty f(E)\mathrm{d}E} \tag{1}$$

here E, k, are the energy of the electrons and the Boltzmann constant, respectively.

The ion density is determined by three methods: (1) from the probe-sheath theory of Allen, Boyd and Reynolds ($N_{i\mathrm{ABR}}$) [17], (2) from the theory of Chen [18] ($N_{i\mathrm{Vf}}$) and (3) from the probe theory of Bernstein, Rabinowitz and Laframboise (N_i) [15, 19]. At a distance of 19 cm from the outlet of the cathode, plasma parameters were also measured with a flat probe, diameter 2 mm. Ion density was calculated using Sheridan's theory [20].

3. Results

3.1. Plasma and floating potentials

Figure 3 shows the plasma potential U_s, floating potential U_f, and electron temperature T_e as a function of a distance from the magnetron. The edge of the cathode has coordinate $Z = 0$. The plasma and floating potentials are negative inside the cathode, while near the mouth they increase to positive values and then reach a plateau.

Inside the cathode the magnitude of the plasma potential is minus tens of volts, and radial and longitudinal electric field strengths are about 2–6 V cm. The electric field peaks at

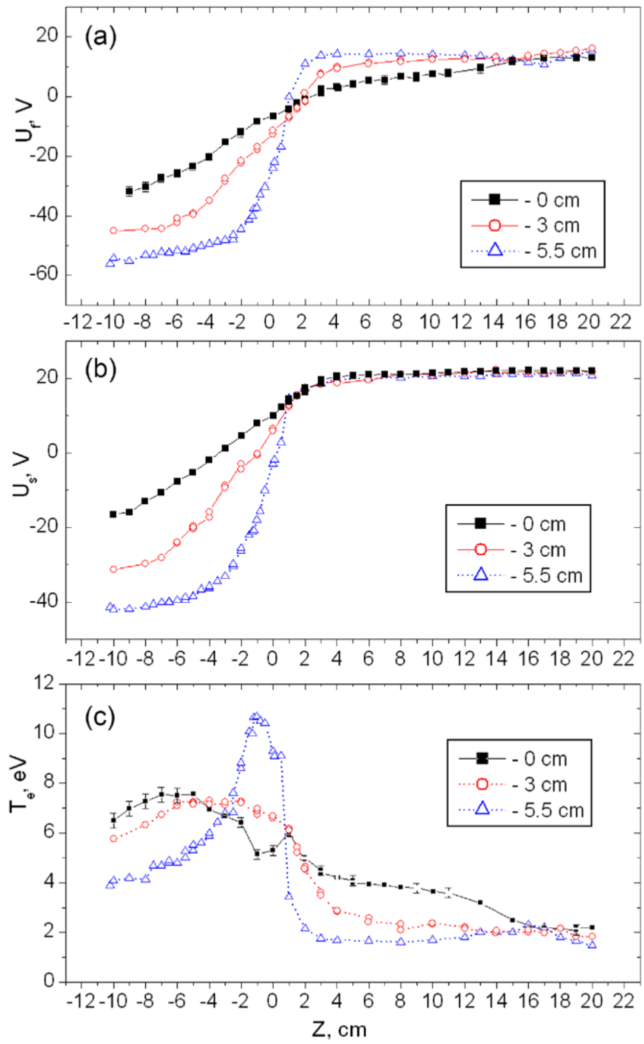

Figure 3. The distribution along Z axis of: (a) floating potential U_f; (b) plasma potential U_s; (c) electron temperature T_e. 10 mTorr, 50 sccm, $I_{el} = 3.5$ A, $W = 2.2$ kW.

$15\,\mathrm{V\,cm^{-1}}$ at a radius of 5.5 cm, near the outlet of the cathode. A potential well retards ions inside the magnetron. Conversely, electrons are accelerated by the electric field and ions stream out behind them.

It should be noted that the positive voltage on the anode ring increases the floating and plasma potentials at the same value everywhere, including inside the cathode region.

3.2. Electron temperature

The electron temperature on the axis increases from 6.5 to 7.5 eV inside the cathode at $-10\,\mathrm{cm} < Z < -6\,\mathrm{cm}$, then decreases to 5 eV closer to the exit of the cathode. Outside the cathode T_e slowly reduces to 4 eV at $Z = 4$ cm, then remains nearly constant up to $Z = 8$ cm, further decreasing to 2 eV.

At a radius of 3 cm the dependence of T_e on Z is similar to the function $T_e(z)$ at radius $R = 0$. At a radius of 5.5 cm the electron temperature increases slowly first from 4 eV at $Z = -10$ cm, and then rises sharply and reaches a maximum of 11 eV at $Z = -1$ cm. Once outside the cathode T_e reduces abruptly to plateau at about 1.8 eV. Near the anode ring

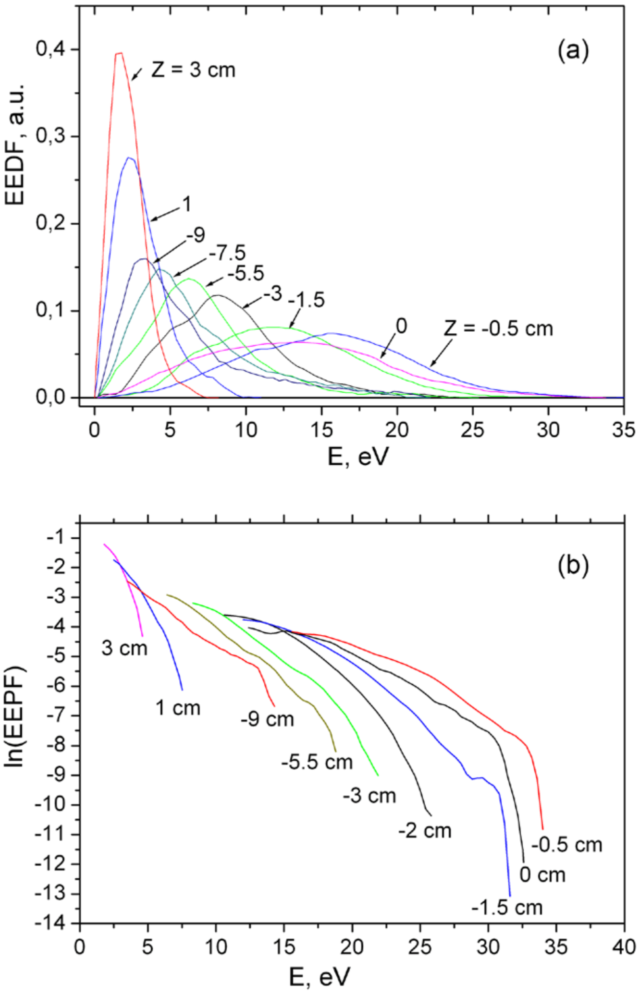

Figure 4. (a) Normalized EEDF and (b) EEPF measured at different distances along Z axis at $R = 5.5$ cm.

(14 < Z < 17 cm) T_e increases to 2.2 eV. The high values of electron density and temperature at this distance allow effective ionization of sputtered metal atoms from the target to the substrate.

3.3. Electron energy distribution function

Figure 4(a) presents the normalized EEDF (the area below the curve is equal to 1) measured at different distances along the Z axis at radius $R = 5.5$ cm. Here we enter the outer part of the ionization region. The electrons in this region have a high energy. In the region $-7.5 < Z < -0.5$ cm the EEDF peak position increases from 4 to 16 eV, then the maximum shifts sharply to 2.2 eV at $Z = 1$ cm. Recall that the ionization energies of argon and copper are 15.7 and 7.73 eV respectively.

The electron energy probability functions (EEPF) obtained by dividing $f(E)$ from figure 4(a) by $\sqrt{E}$ are shown in figure 4(b) on the semilogarithmic scale (displayed only the falling branch of its curve). This function is convenient because, for a Maxwellian distribution, its logarithm depends linearly on the electron energy [21]. The two-temperature EEDF is not observed. Electrons of highest energy (up to 25–35 eV) are located near the magnetron mouth in the range -2.5 cm $< Z < 0$ cm. In this region the electron energy distribution function appears to be closer to a Druyvesteinlike EEDF.

Deep inside ($-9 < Z < -5$) and outside the cathode the EEDF is close to a Maxwellian distribution. The tail of the curves abruptly cut off due to low signal-to-noise ratio.

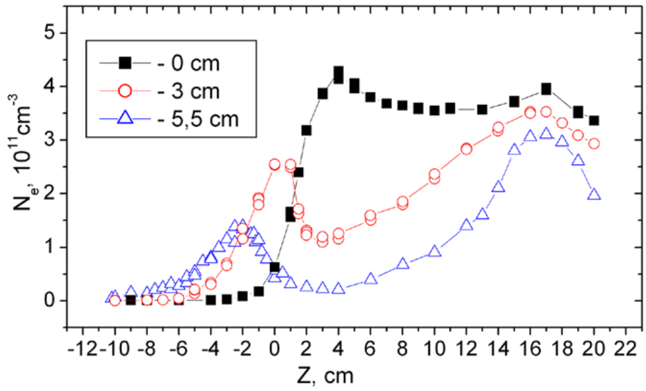

Figure 5. The electron density distribution along Z axis at different radii.

3.4. Electron and ion densities

Figure 5 shows the longitudinal distribution electron density N_e. The electron density drops to a low value when entering the cathode ($Z < 0$) at radius 0 cm. Outside the hollow cathode, near the axis the electron density increases sharply to a value of $4.2 \cdot 10^{11}$cm^{-3} at $Z = 4$ cm and then has a small drop. At $Z = 17$ cm, the electron density has a second maximum of $3.9 \cdot 10^{11}$ cm^{-3}.

The electron density at a radius of 3 cm begins to increase and reaches a maximum value of $2.5 \cdot 10^{11}$ cm^{-3} at $Z = 0.5$ cm outside the cathode. Then it falls to 10^{11} cm^{-3} at $Z = 3$ cm after which N_e increases and has a second maximum of $3.5 \cdot 10^{11}$ cm^{-3} at $Z = 17$ cm.

At a radius of 5.5 cm the electron density begins to grow inside the cathode and reaches a maximum value of $1.4 \cdot 10^{11}$ cm^{-3} at $Z = -2$ cm, and then decreases towards the exit of the cathode. At this radius we enter into the ionization region where the secondary electrons are captured. The probe disturbs discharge in this zone and the discharge voltage rises by 5%. The racetrack occupies the region -7 cm $< Z < -1$ cm and highest erosion is at $Z = -3$ cm.

Further, the electron density decreases to 10^{10} cm^{-3} at $Z = 3$ cm then increases smoothly to a peak of $3 \cdot 10^{11}$ cm^{-3} at $Z = 17$ cm where an anode ring is located. The magnitude of the electron density at the second maximum at $R = 5.5$ cm is twice as strong as the first maximum, inside the cathode. Note that radial uniformity of the electron density also rises also at this location.

The second maximum is rather narrow and N_e sharply falls to $2 \cdot 10^{11}$ cm^{-3} at $Z = 20$ cm. Thus, the use of the anode ring creates a local increase in density.

Since magnetic field affects the electrons, we have also measured the ion density. Calculations show that the density distribution of ions is similar to that of electrons, but the

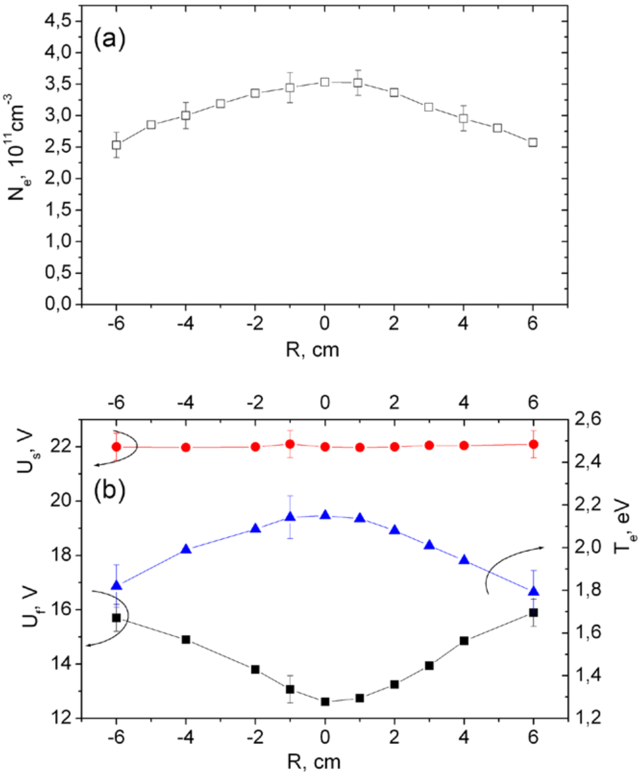

Figure 6. Radial profiles of: (a) the electron density N_e; (b) electron temperature T_e, floating U_f and plasma U_s potentials. 19 cm from the target.

magnitude of N_{iABR} is some 10% greater than N_e, and values of N_{iVf} and N_i are about 1.5 and 2 times greater than N_e, respectively.

To verify the results of longitudinal measurements by a cylindrical probe we measured the ion density by a flat probe at $Z = 19$ cm.

Figure 6 shows the radial distribution of the ion density, plasma and floating potentials and the electron temperature at a distance of 19 cm from the cathode. The ion density was measured using a flat probe. The ion density has pool uniformity at electromagnet current of $I_{el} = 3.5$ A.

On the axis the electron temperature T_e has maximum value 2 eV. At the radius $R = 6$ cm it reduces to 1.8 eV. The electrons with higher energy are located on the discharge axis, so their temperature is high.

Despite the significant nonuniformity of plasma density, plasma potential U_s varies only slightly along the radius. Floating potential U_f in the center of the discharge takes the minimum value as here are the highest concentration of high-energy electrons.

Measurements of plasma density along the radius are in quite good agreement with results of longitudinal measurements.

Plasma density distribution inside the cathode ($-9 < Z < 0$) varies little even when additional magnets are installed behind the magnetron and sputtering arises from the rear surface of the cathode.

The position of the maximum and the width of the racetrack depend on the magnitude of the magnetic field and discharge current. When they grow, the peak shifts to the mouth of the cathode and the width increases, which can be attributed to the force of $I_\varphi x\, B_r$. A detailed discussion of these measurements is beyond the scope of this paper.

4. Discussion

In the magnetron, the highest-density plasma is located in the ionization area near the side surface. Here, the magnetic field captures secondary electrons emitted from the cathode, which produce an ionization of the buffer gas and sputtering atoms of the target. Crossed $E \times B$ fields cause electron drift in an azimuthal direction, with the result that inside the hollow cathode, high-density plasma is generated near the side surface. In our magnetron, the magnetic field is strong (450 gauss) and the layer thickness is small.

Using the Bohm flux formula the ion density near the cathode ring can be estimated:

$$j_i = 0.6eN_i\sqrt{\frac{T_e}{M_i}}. \tag{2}$$

The ion current density is:

$$j_i = \frac{I}{2\pi Rw}. \tag{3}$$

For mean width erosion track $w = 6$ cm, cathode radius $R = 7$ cm and discharge current $I = 7$ A we find $j_i = 22.7$ mA cm^{-2}. For $T_e = 6$ eV we obtain $N_i \approx 6.2 \cdot 10^{11}$ cm^{-3}. This value is much greater than was measured at radius 5.5 cm. Thus at the radius of 5.5 cm we enter into the outer part of the ionization region. Discharge could be seen through the window at the far end of the chamber. Visually, the ionization zone near the cylindrical surface of the target has a thickness of about 5–7 mm. Probe measurements to a larger radius have been hampered because of strong perturbation of the discharge and breakdowns on the probe.

Figure 5 shows that the plasma is formed near the side walls of the cathode. At the exit of the cathode, the plasma density at the radius $R = 5.5$ cm decreases sharply. Here the electrons cannot escape, due to the large radial magnetic field.

A similar pattern occurs for radius of 3 cm. The first peak of electron density at a radius of 3 cm is higher than the peak at radius 5.5 cm. Here, electron density increases as a result of the electrons coming from the depths of the cathode, and also due to additional ionization. Subsequent reduction of electron density indicates that it is difficult for electrons to escape from the cathode along this radius.

Low plasma density near the axis inside the cathode can be explained by rapid escape of the plasma through the region of weak magnetic field at $R = 0$. At the outlet of the cathode there is a quite strong electric field $E_z = -\partial U_p/\partial z$ (figure 4(*b*)). This field accelerates the electrons, which pull ions behind themselves by ambipolar diffusion. An additional source that can enhance the electron flow in the axial direction can be caused by the axially diverging magnetic field, i.e. the magnetic mirror force. Under an axially diverging magnetic field, electrons are axially accelerated by the magnetic mirror force, which is represented by [21]:

$$F_z = -\frac{m_e v_\perp^2}{2B_z}\frac{\partial B_z}{\partial z}. \tag{4}$$

Here $v_\perp$ is the component of the electron velocity perpendicular to the magnetic field. This force F_z pushes an electron into regions of smaller B.

The electric field E_z just behind the cusp is reduced and the plasma is retarded. This leads to a strong increase of plasma density at $R = 0$. Additional contribution to the increase in plasma density causes ionization due to rather high electron temperature.

It is seen from figure 5 that downstream the cusp plasma expands to more radial uniformity due to defocussing of the plasma by the electromagnet. Magnetized electrons move along divergent magnetic field lines of the electromagnet to the anode ring at $Z = 17$ cm. Here they are captured by the magnetic trap located around the anode ring. The electrons transmitted from the cathode are confined by the crossing electrical and magnetic fields, creating an azimuthal current and forming a region of high-density plasma. As mentioned above, electron temperature rises in this area. Without magnets around the anode rings, the plasma density is reduced by one half at this location [12]. Figure 5 shows that plasma density increases greatly at large radii. Thus the magnetic trap placed around the anode ring strongly increases the ionization in the region of its location.

These measurements raise the question: where is there a large ionization of sputtered metal atoms? Recall that for the same parameters of discharge, the ionization fraction of the Cu flux cm reaches 25% at $Z = 19$ cm [12]. Inside the cathode the layer of dense plasma is thin and probability of ionization of the metal atoms is small. Therefore, the main ionization of sputtered atoms takes place outside the cathode, where the high density plasma exists in a large volume.

Preliminary measurements using an optical probe confirm this assumption. The probe is a ceramic tube 74 cm long with an internal diameter of 9 mm and a quartz window at the end that is remote from the plasma. Moving the probe along the Z axis, the average radiation from the emission cone in front of the probe can be measured. The radiation of various spectral lines can be detected with a monochromator. At the axis ($R = 0$) the intensity of Cu^+ (213.6 nm) increases 25 times for $Z = 11$ cm (end of the cathode) and $Z = 28$ cm respectively. At $R = 6$ cm the intensity of this line increases three-fold. For the copper atom line (Cu216, Cu 218 nm) this ratio is equal to 3.

Axial distribution of floating U_f and the plasma U_s potential (figures 3(*a*) and (*b*)) is similar to that for HIPIMS [22]. Such distribution acts as a potential barrier for ions, which prevents their exit from the cathode. This results in a decrease in the rate of deposition, since the bulk density of the sputtered metal atoms is located inside this trap. In our case the deposition rate is large enough (100 nm min^{-1}) at $Z = 19$ cm for 2.2 kW power and 10 mTorr pressure [12]. This also speaks in favor of our assumption that the main ionization of copper atoms takes place outside of the cathode, where the potential barrier is small.

Attention is drawn to a large increase in the temperature and the energy of the electrons leaving the cathode at $R = 5.5$ cm (figures 3 and 4). In the region $-1 < Z < 0.5$ cm energy of the electrons increases sharply and there are electrons with energies up to 30 eV. This implies the existence of a source for electron heating. The mechanism of this phenomenon is not clear. It can be assumed that the spike in temperature is due to the $E \times B$ rotation of electrons. Although ions are not magnetized, the azimuthal electric field E_φ will pull ions and they will also rotate. Traces of such rotation can be seen on the walls of the chamber. This question requires further study.

It is interesting to compare our experimental data with the results of the computer simulation in [2]. In this article, results from a 2D computational investigation of HCM are discussed in which the geometry of the magnetic field inside the cathode is quite similar to ours. Most of the calculations were carried out for magnetic field magnitude 80 gauss, but also include the results for magnetic field 500 gauss. Calculations revealed that the plasma parameters depend strongly on the location of the cusp in the magnetic field. Our measurements were carried out when the cusp was located at the target opening. According to calculations, the maximum plasma density in this case takes place adjacent to the target surface closer to the mouth, corresponding to the peak in electron temperature at those locations. The electron density on the axis is much less than maximum value. The electric and magnetic fields being parallel at the target opening allows electrons to escape the hollow cathode region. These results are in agreement with our data inside the target. Outside the cathode our electron density results differ from those calculated. Probe measurements showed that plasma density on the axis sharply increases directly outside the cathode. Thus the maximum plasma density is achieved behind the cusp. According to the results of modeling [2] the electron density decreases monotonically downstream. We consider that the phenomena in plasma of HCM are very complex and computer modelling could not take into account all suv phenomena.

5. Conclusion

Using probe measurements, the plasma parameters inside and outside a hollow cathode magnetron with discharge power 2.2 kW and pressure of 10 mTorr have been determined. The magnetic field of the HCM is 400 gauss. It was found that inside the cathode high plasma density occurs near the side surface of the cathode in the ionization region. The plasma density on the axis is lower. The EEDF shows the presence of electrons with energy up to 30 eV. The measurements showed that ionization occurs not only within the cathode but also to a large extent downstream. The magnetic trap placed around the anode ring increases the density and homogeneity of the plasma several times in the region of its location. This makes possible a plasma with density greater than 10^{11} cm^{-3} at discharge power 2 kW at a distance of 20 cm from the cathode.

Acknowledgment

This work was supported by the Center for Collective Use 'Plasma Technology of Micro and Nanofilms'.

References

[1] Klawuhn E, D'Couto G C, Ashtiani K A, Rymer P, Biberger M A and Levy K B 2000 *J. Vac. Sci. Technol.* **18A** 1546
[2] Vyas V and Kushner M J 2006 *J. Vac. Sci. Technol.* **24A** 1955
[3] Hopwood J and Qian F 1995 *J. Appl. Phys.* **78** 758
[4] Hopwood J 1998 *Phys. Plasmas* **5** 1624
[5] Rossnagel S M 2003 *J. Vac. Sci. Technol.* **21** 74
[6] Gorbatkin S M and Rossnagel S M 1996 *J. Vac. Sci. Technol.* **14B** 1853
[7] Gudmundsson J T 2010 *Vacuum* **84** 1360
[8] Anders A 2011 *Surf. Coat. Technol.* **205** S1–9
[9] Kozák T, Vlček J and Kos Š 2013 *J. Phys. D: Appl. Phys.* **46** 105203
[10] Meng L, Raju R, Flauta R, Shin H and Ruzic D N 2010 *J.Vac. Sci. Technol.* **28A** 112
[11] Wu L, Ko E, Dulkin A, Park K J, Fields S, Leeser K, Meng L and Ruzic D N 2010 *Rev. Sci. Instrum.* **81** 123502
[12] Tsar'gorodsev Yu P, Poluektov N P, Usatov I I, Evstigneev A G and Kamyschov I A 2014 *Plasma Phys. Rep.* **40** 754
[13] Rubinstein J and Laframboise J G 1978 *Phys. Fluids* **21** 1655
[14] Sheridan T E, Goeckner M J and Goree J 1998 *J. Vac. Sci. Technol.* **16A** 2173
[15] Laframboise J G 1966 *Report No* 100 Toronto Institute for Aerospace Studies University of Toronto
[16] Mausbach M 1997 *J. Vac. Sci. Technol.* **15A** 2923
[17] Allen J E, Boyd R L F and Reynolds P 1957 *Proc. Phys. Soc.* **70B** 297
[18] Chen F F 1965 *J. Nucl. Energy* **Pt.C** 747
[19] Bernstein I B and Rabinowitz I 1959 *Phys. Fluids* **2** 112
[20] Sheridan T E 2010 *J. Phys. D: Appl. Phys.* **43** 1
[21] Lieberman M A and Lichtenberg A J 1994 *Principles of Plasma Discharges and Materials Processing* (New York: Wiley)
[22] Mishra A, Kelly P J and Bradley J W 2010 *Plasma Sources Sci. Technol.* **19** 1